Least-squares joint imaging of multiples and primaries

Morgan Brown* and Antoine Guitton**

**Formerly Department of Geophysics, Stanford University, Stanford, CA 94305-2215,*

Currently Amerada Hess Corporation, 500 Dallas St., Houston, TX 77002

***Department of Geophysics, Stanford University, Stanford, CA 94305-2215*

(March 14, 2005)

ABSTRACT

Multiple reflections contain subsurface reflectivity information which often complements that found in primary reflections. Previous attempts to combine the additional information by summing prestack images of the primaries and multiples have generally failed because of crosstalk leakage between the images. We present a general linear least-squares inversion method, Least-Squares Joint Imaging of Multiples and Primaries (LSJIMP), to simultaneously suppress crosstalk noise and combine pegleg multiples and primaries in a prestack sense. In general, LSJIMP is compatible with a wide variety of prestack imaging methods and can be extended to jointly image primaries and other embedded wave modes like shear wave conversions.

We present a particular LSJIMP implementation which utilizes an efficient linear operator to model and image pegleg multiples in a "true relative amplitude" sense. Applied to a given type of pegleg multiple in the data, our imaging operator produces an image directly comparable to primaries after normal moveout (NMO). Our operator's kinematic component is an extension of the NMO equation which independently images "split" peglegs in a moderately heterogeneous Earth. Its amplitude component corrects multiples for their differences in angle-dependent reflection strength

and illumination, relative to a primary. We test our LSJIMP implementation on 2D and 3D prestack field data examples and show that the method cleanly separates primaries and multiples and also uses the joint information in the events to interpolate signal in acquisition gaps.

INTRODUCTION

Seismic data acquired in marine environments almost always contain observable multiple reflections from the air-water interface. Multiples may significantly impede the construction and interpretation of an image of the primaries, especially in regions with strong reflectors (e.g., "hard" water bottom or salt bodies). Multiple suppression techniques have, by necessity, advanced contemporaneously with reflection imaging for many years.

Despite its usual classification as noise, however, energy from multiples often penetrates deeply enough into the earth to illuminate the prospect zone. In this sense, the multiples can be viewed as perfectly viable signal, rather than as noise. Moreover, since they illuminate different angular ranges and reflection points (see Figure 1), a primary and its multiples are more than simply redundant. In theory and in practice, multiples provide subsurface information not found in the primaries.

To actually use the new information provided by multiples, the multiples and primaries must first be mapped to a domain where they are directly comparable, and then combined in some fashion. Imaging algorithms like migration reduce the signal – either primaries or multiples – to a compact form by removing the effects of wave propagation through the overburden. Additionally, if the prestack primary and multiple images are arranged in angle-domain common-image gathers (e.g., Sava and Fomel (2003)), the events can be jointly analyzed for angle-dependent phenomenon. Thus the angle domain after prestack imaging represents a natural domain in which to combine multiples and primaries.

An important class of multiple suppression techniques predict the multiples by "adding a multiple bounce" to the recorded data by wavefield extrapolation (Morley 1982; Berryhill and Kim 1986; Wiggins 1988; Lu et al. 1999) or by autoconvolution (Riley and Claerbout 1976; Tsai 1985; Verschuur et al. 1992). Conversely, reversing the extrapolation direction "removes a multiple bounce" from the data and transforms pegleg multiples into pseudo-primary events (Berkhout and Verschuur 2003; Shan 2003). While conventional migration can image the pseudo-primaries (Shan 2003), most published multiple imaging techniques perform the reverse modeling process implicitly, and image the multiples directly with Kirchhoff (Reiter et al. 1991; He and Schuster 2003) or wave equation (Berkhout and Verschuur 1994; Yu and Schuster 2001; Guitton 2002) migration.

While these techniques correctly image multiples to the position of an equivalent primary, they fail to seriously tackle the equally important problem of combining the multiple and primary images. Primaries and each mode of multiple constitute semi-independent measurements of the earth's reflectivity, but unfortunately overlap one another in a single data record. Summing the primary and multiple images (Reiter et al. 1991; Berkhout and Verschuur 1994; Shan 2003) could potentially improve signal-to-noise ratio and fill illumination gaps, but this strategy encounters a significant problem. Just as multiples constitute noise on the primary image, primaries and higher order multiples constitute noise on the first-order multiple image, as shown on Figure 2. We refer to these events which contaminate each image as "crosstalk" (Claerbout 1992). Corresponding crosstalk events on the primary and multiple images have similar kinematics, so summing the images will do little to to increase signal-to-noise ratio or improve signal fidelity, unless the individual modes are separated prior to imaging and combination. Unfortunately, cleanly separating a variety of different multiple modes from prestack data is both expensive and difficult. Moreover, if the mode separation is performed as a preprocessing step, amplitude bias in the separated modes will likely inhibit the later integration of primaries and multiples.

In this paper we introduce the LSJIMP (Least-squares Joint Imaging of Multiples and Primaries) method, which aims to solve the separation and integration problems simultaneously, as a global least-squares inversion. The model space of the inverse problem, illustrated in Figure 3, consists of images corresponding to primaries and to each important multiple mode. Correct partitioning of the energy from each mode into one, and only one image, implies a) that multiples and primaries have been separated, and b) that the modeled data fits the recorded data. However, as the inverse problem is under-determined, minimization of the modeling error alone does not ensure a correct partitioning of energy, since forward-modeled crosstalk is indistinguishable from forward-modeled signal (see Figure 4). To overcome this problem, we devise three model regularization operators which discriminate crosstalk from signal and thereby properly partition each mode's energy into the correct image.

The model regularization operators serve a higher purpose than crosstalk suppression alone, however, and represent the novelty of the LSJIMP method. Differential operators applied across reflection angle and between images "spread" signal from other angles or images to fill illumination gaps and increase signal fidelity. By exploiting an additional, previously ignored dimension of data redundancy – that between primaries and multiples – we can, with a degree of rigor, claim to have solved a "joint imaging" problem and to actually have used the multiples constructively. LSJIMP's use of multiples to constrain the least-squares imaging problem is a novel generalization of existing regularized least-squares prestack imaging schemes which exploit signal redundancy across reflection angle to fill illumination gaps (Kuehl and Sacchi 2001; Prucha-Clapp and Biondi 2002; Wang et al. 2003).

THE LSJIMP INVERSE PROBLEM

Generalizing the LSJIMP forward model from Figure 3, we conceptualize the recorded data as the superposition of primary reflections and p orders of pegleg multiples from n_{surf} multiple-generating surfaces. In Figure 3, $p = 1$ and $n_{\text{surf}} = 1$. Whereas a first-order pegleg splits into source-side and receiver side legs, an i^{th} order pegleg splits into $i+1$ legs. Denoting the primaries as $\mathbf{d}_0$ and the k^{th} leg of the i^{th} order pegleg from the m^{th} multiple generator as $\mathbf{d}_{i,k,m}$, the modeled data takes the following form:

$$\mathbf{d}_{\text{mod}} = \mathbf{d}_0 + \sum_{i=1}^{p} \sum_{k=0}^{i} \sum_{m=1}^{n_{\text{surf}}} \mathbf{d}_{i,k,m}. \tag{1}$$

We can cast the $\mathbf{d}_{i,k,m}$ as linear functions of prestack images. Let us denote the modeling operator for primaries $\mathbf{L}_0$ and the image of the primaries $\mathbf{m}_0$. Similarly, for the pegleg $\mathbf{d}_{i,k,m}$, we denote the modeling operator and image $\mathbf{L}_{i,k,m}$ and $\mathbf{m}_{i,k,m}$, respectively. We can now rewrite equation (1):

$$\begin{aligned} \mathbf{d}_{\text{mod}} &= \mathbf{L}_0\mathbf{m}_0 + \sum_{i=1}^{p} \sum_{k=0}^{i} \sum_{m=1}^{n_{\text{surf}}} \mathbf{L}_{i,k,m}\mathbf{m}_{i,k,m}, & (2) \\ &= \mathbf{L}\mathbf{m}. & (3) \end{aligned}$$

It is important to note that signal events in $\mathbf{m}_0$ and in the $\mathbf{m}_{i,k,m}$ are assumed consistent with respect both to kinematics and to angle-dependent amplitudes. This assumption implies that signal events are comparable between images, and thus implies that the $\mathbf{L}_{i,k,m}$ must be "true amplitude" modeling operators, relative to $\mathbf{L}_0$.

The LSJIMP method optimizes (e.g., using the conjugate gradient method) the primary and multiple images by minimizing the ℓ_2 norm of the data residual, defined as the difference between the recorded data, $\mathbf{d}$, and the modeled data:

$$\min_{\mathbf{m}} \ \|\mathbf{W_d}\,[\mathbf{d} - \mathbf{L}\mathbf{m}]\,\|^2, \tag{4}$$

where the residual weighting operator, $\mathbf{W_d}$, forces the residual to be independent and identically dis-

tributed (iid), or more intuitively, uncorrelated and evenly scaled. Even simpler choices are possible; in our LSJIMP implementation, we chose $\mathbf{W_d}$ as a diagonal weighting operator (0.0 at missing trace locations, 1.0 elsewhere).

Other authors have solved a similar least-squares problem. Nemeth et al. (1999) jointly imaged and separated compressional waves and various (non-multiple) embedded coherent noise modes. Guitton et al. (2001) used a prior multiple model and nonstationary prediction-error filters to model primaries and surface-related multiples.

Minimization (4) is generally under-determined, implying infinitely many "optimal" solutions. The non-uniqueness problem is closely related to crosstalk leakage, as illustrated by Figure 4. Recall that all energy from pegleg $\mathbf{d}_{i,k,m}$ must be partitioned to $\mathbf{m}_{i,k,m}$ if we hope to meaningfully combine the primary and multiple images. To better constrain the LSJIMP inversion, we regularize the problem.

LSJIMP Regularization

Quite simply, an under-determined minimization problem has more unknowns than equations – model regularization consists of adding unique equations to the system. More rigorously, the model regularization is closely related to the prior model covariance, or how we believe model parameters depend on one another (Tarantola 1987). Figure 3 motivates the desired model covariance for the LSJIMP problem: after optimization, the primary and multiple images should contain only energy from one particular primary or multiple mode. In other words, the images should be crosstalk-free.

We can rewrite minimization (4) after adding a generic linear model regularization operator, $\mathbf{R}$:

$$\min_{\mathbf{m}} \ \|\mathbf{W_d}\,[\mathbf{d}-\mathbf{Lm}]\,\|^2+\epsilon\|\mathbf{Rm}\|^{\mathbf{2}}. \tag{5}$$

We call the second term of equation (5) the model residual. Scalar ϵ balances the relative importance of the data and model residuals in the minimization. If we design $\mathbf{R}$ to (counterintuitively) boost

unwanted components of $\mathbf{m}$, then in order to minimize (5), a solver will tend to suppress those components.

We add three model regularization operators to the basic LSJIMP inverse problem which boost crosstalk energy relative to signal energy. These operators also exploit the signal's redundancy – within and between images – to increase signal fidelity and fill illumination gaps and missing traces.

- **Differencing across angle** - After prestack imaging with the correct velocity, signal events are flat with angle/offset, while crosstalk events generally have residual moveout. Provided that the signal's amplitude-versus-angle response varies slowly, a differencing operator applied across angle tends to boost crosstalk amplitude, but not signal amplitude. We denote this operator $\mathbf{D_h}$. Other authors have used a similar methodology to penalize illumination gaps in least-squares prestack migration (Kuehl and Sacchi 2001; Prucha-Clapp and Biondi 2002; Wang et al. 2003).

  If a signal event is not flat, $\mathbf{D_h}$ will damage it in the LSJIMP inversion. Conversely, $\mathbf{D_h}$ cannot distinguish crosstalk from signal at near angles/offsets, where both events are usually flat.

- **Differencing between images** - After prestack imaging, signal events on the primary and multiple images are by definition consistent with respect to kinematics and amplitudes. Conversely, corresponding crosstalk events on two images (e.g. first-order multiples on $\mathbf{m}_0$ and second-order multiples on $\mathbf{m}_{1,k,m}$) generally have different residual moveout. The moveout differences are generally small at near angles/offsets, but increase at far offsets and in the presence of subsurface complexity (Brown 2004). Where the moveout differences are larger than a quarter wavelength, a differencing operator applied between images tends to boost crosstalk amplitude, but not signal amplitude. We denote this operator $\mathbf{D_m}$.

  A central motivation for LSJIMP is the desire to combine information from the multiple and primary images by averaging. As a regularization operator, $\mathbf{D_m}$ accomplishes the averaging, by

penalizing differences between images. Additionally, because the averaging occurs within the framework of a least-squares minimization, we can both combine the multiples and primaries and quantitatively fit the data.

In using $\mathbf{D_m}$, we assume that signal events on all images are perfectly consistent. Imperfections in the modeling operator, $\mathbf{L}_{i,k,m}$, lead to differences in the signal events, which violate this assumption and cause $\mathbf{D_m}$ to damage signal events.

Both the primary and multiple images have acquisition gaps. When implementing LSJIMP, $\mathbf{D_m}$ should be supplemented with an appropriate diagonal weighting operator which reflects the local information content of an image. For example, at far angles/offsets, multiples usually carry little information, so the weighting operator would nullify the output of $\mathbf{D_m}$ there.

- **Crosstalk penalty weights** - Given a prior signal estimate, $\mathbf{m}^{[p]}_{i,k,m}$, we can directly model the expected crosstalk events on all the $\mathbf{m}_{i,k,m}$. Applying $\mathbf{L}_{i,k,m}$ to $\mathbf{m}^{[p]}_{i,k,m}$ yields an estimate of the $\{i,k,m\}$ pegleg. Imaging this estimated pegleg as if it was a different multiple, say by applying $\mathbf{L}^T_{i',k',m'}$, in turn yields an estimate of the crosstalk from the $\{i,k,m\}$ multiple on $\mathbf{m}_{i',k',m'}$. We then sum over all $\{i,k,m\}$ to obtain the total estimated crosstalk on $\mathbf{m}_{i',k',m'}$, which we denote $\mathbf{m}^{[c]}_{i',k',m'}$:

$$\mathbf{m}^{[c]}_{i',k',m'} = \sum_{i=i_0}^{p}\sum_{k=0}^{i}\sum_{m=1}^{n_{\text{surf}}} \mathbf{L}^T_{i',k',m'}\mathbf{L}_{i,k,m}\mathbf{m}^{[p]}_{i,k,m}, \text{ where } k \neq k',\ m \neq m' \text{ and } i_0 = \begin{cases} 1 & \text{if } i' = 0 \\ i & \text{otherwise} \end{cases} \tag{6}$$

We convert each $\mathbf{m}^{[c]}_{i',k',m'}$ into a diagonal weighting function by computing the absolute value. We denote this operator $\mathbf{D_c}$. While $\mathbf{D_h}$ and $\mathbf{D_m}$ tend to suppress crosstalk at far angles only, $\mathbf{D_c}$ suppresses crosstalk at all angles.

Strictly speaking, we lack a prior signal estimate without performing a nonlinear iteration (Brown 2004). However, between the seabed reflection and its first multiple, the recorded data

effectively contain only primaries, so we can limit the crosstalk prediction to events arising from multiple generators above the first seabed multiple. This assumption particularly applies to deepwater marine data.

Although the crosstalk weights overlap (and damage) signal events on any image, the previous two regularization operators ($\mathbf{D_h}$ and $\mathbf{D_m}$) "spread" redundant signal information from other images and other angles/offsets to compensate for any losses. Figure 5 illustrates the application of the crosstalk weights to the primary image, $\mathbf{m}_0$. The weights cleanly boost the energy of the crosstalk events (multiples).

We can now rewrite the general regularized LSJIMP minimization (5) using the three regularization operators:

$$\min_{\mathbf{m}} Q(\mathbf{m}) = \|\mathbf{W_d}\,[\mathbf{Lm}-\mathbf{d}]\|^2 + \epsilon_1^2\|\mathbf{D_h m}\|^2 + \epsilon_2^2\|\mathbf{D_m m}\|^2 + \epsilon_3^2\|\mathbf{D_c m}\|^2. \tag{7}$$

Effectively, $\mathbf{R}$ in equation (5) is replaced by the column operator $[\mathbf{D_h}\ \mathbf{D_m}\ \mathbf{D_c}]^{\mathbf{T}}$, while ϵ_1, ϵ_2, and ϵ_3 replace ϵ. A method for quantitatively choosing ϵ_1, ϵ_2, and ϵ_3 remains a subject of research. Qualitatively, high values lead to good crosstalk suppression and some damage to signal events, while low values lead to good signal preservation and poor crosstalk suppression.

PARTICULAR LSJIMP IMPLEMENTATION

In this section we present a particular LSJIMP implementation which utilizes an efficient linear operator to model and image pegleg multiples in a true relative amplitude sense. Applied to primary reflections after NMO, the forward operator models a particular pegleg. Applied to that particular pegleg in the data, the adjoint operator produces events which are directly comparable to primaries after NMO. The operator's kinematic component is an extension of the NMO equation which images

"split" peglegs. Its amplitude component corrects multiples for their differences in angle-dependent reflection strength, relative to a primary.

Kinematic pegleg imaging in a 1D Earth

In a laterally-homogeneous earth, the NMO equation describes a primary's traveltime as a function of source-receiver offset:

$$t = \sqrt{\tau + \frac{\|\mathbf{x}\|^2}{V_{\text{rms}}^2(\tau)}}. \tag{8}$$

Applied as an offset-dependent time shift, equation (8) flattens a primary (on a CMP gather) with offset vector $\mathbf{x}$ and root-mean-square (RMS) velocity $V_{\text{rms}}(\tau)$ to its zero-offset traveltime, τ.

Figure 6 motivates an analogous NMO equation for pegleg multiples. Kinematically, a first-order pegleg can be conceptualized as a "pseudo-primary" with the same offset, but with an additional zero-offset traveltime, τ^*, to the multiple generator. We can generalize this intuition to write an NMO equation for an n^{th}-order pegleg.

$$t = \sqrt{(\tau + n\tau^*)^2 + \frac{\|\mathbf{x}\|^2}{V_{\text{eff}}^2}}, \quad \text{where} \tag{9}$$

$$V_{\text{eff}}^2 = \frac{\left(n\tau^* V_{\text{rms}}^2(\tau^*) + \tau V_{\text{rms}}^2(\tau)\right)}{\tau + n\tau^*}. \tag{10}$$

V_{eff}, the pseudo-primary's effective RMS velocity, can be easily derived (Wang 2003) from the definition of RMS velocity. The relative shift of the primary and pegleg reflection points (Δy in Figure 6) decreases asymptotically to zero for $\tau \to \infty$ from a maximum value at the seabed.

Amplitude corrections for peglegs

Primaries and multiples recorded at fixed offset follow different raypaths from source to receiver, and thus exhibit different amplitude-versus-offset (AVO) behavior and suffer different attenuation and

geometric spreading losses. We present two operators that normalize (relative to a primary) a pegleg for these effects, and a reflection operator that accounts for a multiple's extra bounces.

- Figure 7 illustrates that in a $v(z)$ medium there exists a vector $\mathbf{x}_p$ such that a pegleg with offset $\mathbf{x}$ and primary with offset $\mathbf{x}_p$ are invariant with respect to AVO and, ignoring attenuation above the multiple generator (this is often water), also to attenuation. Noting that the multiple and primary in Figure 7 have the same emergence angle, and thus the same time dip, at $\mathbf{x}$ and $\mathbf{x}_p$, Brown (2004) obtains:

$$\mathbf{x}_p = \frac{\mathbf{x}\tau\, V_{\text{rms}}^2}{\sqrt{(\tau + n\tau^*)^2\; V_{\text{eff}}^4 \;+\; \|\mathbf{x}\|^2 (V_{\text{eff}}^2 - V_{\text{rms}}^2)}} \tag{11}$$

  for a n^{th}-order pegleg. We named the resampling of the offset axis defined by equation (11) "Snell Resampling". Figure 8 illustrates the process on a synthetic CMP gather. The black lines depict the compression of the offset axis and show how energy from the multiples fills the data's coverage gaps.

- Lu et al. (1999) define offset-dependent geometric spreading corrections for a primary (g_{prim}) and its pegleg multiples (g_{mult}):

$$g_{\text{prim}} \;=\; v^* t_{\text{prim}}(\mathbf{x}) = \sqrt{(\tau v^*)^2 + \|\mathbf{x}\|^2 \left(\frac{v^*}{V_{\text{rms}}}\right)^2} \tag{12}$$

$$g_{\text{mult}} \;=\; v^* t_{\text{mult}}(\mathbf{x}) = \sqrt{[(\tau + n\tau^*)v^*]^2 + \|\mathbf{x}\|^2 \left(\frac{v^*}{V_{\text{eff}}}\right)^2}, \tag{13}$$

  where v^* is the surface velocity. We correct a pegleg for geometric spreading by applying $g_{\text{mult}}/g_{\text{prim}}$.

- For simplicity, we assume that a multiple generator's reflectivity varies in space, but not in reflection angle. If $\mathbf{y}$ is the midpoint vector, let us denote $\mathbf{p}(t, \mathbf{x}, \mathbf{y})$ and $\mathbf{q}(t, \mathbf{x}, \mathbf{y})$ as small windows in time, offset, and midpoint around, respectively, a primary and its first pure multiple after

normalized Snell Resampling and differential geometric spreading correction. We optimize the reflection coefficient, $\mathbf{r}(\mathbf{y})$, to minimize the following quadratic functional:

$$\|\mathbf{diag}(\mathbf{p})\,\mathbf{r}-\mathbf{q}\|^2+\epsilon^2\|\nabla_{\mathbf{y}}^2\mathbf{r}\|^2. \tag{14}$$

Operator $\nabla_{\mathbf{y}}^2$ is a 2D Laplacian, operating across midpoint; it imposes a degree of smoothness on $\mathbf{r}(\mathbf{y})$, governed by the tradeoff parameter, ϵ. Using $\mathbf{x}_p$, we can compute the multiple bounce points in a 1D earth for any type of pegleg. A first-order pegleg is scaled by a single reflection coefficient, a second-order pegleg by reflection coefficients from two locations, and so on.

Pegleg Imaging in a moderately heterogeneous Earth

An i^{th}-order pegleg actually consists of $i+1$ unique events. Dipping reflectors cause the events to "split" into individual legs, shown by Figure 9a on field data. Legs with a high apparent velocity hamper Radon demultiple and velocity analysis. Even if not visible, splitting can cause far-offset tuning effects between the legs which introduce a false multiple AVO signature. To accurately model peglegs, therefore, we must extend the previous 1D theory to handle splitting.

Levin and Shah (1977) deduced moveout equations for split 2D peglegs, and Ross et al. (1999) extended the work to 3D. While the equations are exact in a constant-velocity earth, an extension even to $v(z)$ could prove difficult. We present a related earth-model-based imaging method called HEMNO (Heterogeneous Earth Multiple NMO Operator) which can handle variable velocity. In the small dip and constant velocity limit, Brown (2004) shows that HEMNO reduces to Levin and Shah's result.

Figure 10 illustrates HEMNO. When reflectors dip, reflection points move both laterally and vertically. For small dips, the lateral component of reflection point movement is negligible. We can analytically compute the location of a multiple's reflection points in a 1D earth. The basic idea of

HEMNO is to measure the zero-offset traveltimes at the assumed 1D reflection points, then input those measured traveltimes to the 1D NMO for peglegs equation (8). HEMNO requires that the earth not deviate too far from 1D (small dip magnitude, small lateral dip changes, small lateral velocity variation).

If τ_m is the total zero-offset traveltime of the multiple bounces along a pegleg's raypath and τ_p is the zero-offset traveltime of the primary bounce, then we can easily extend equation (8) to HEMNO:

$$t^2 = \left(\tau_m + \tau_p\right)^2 + \frac{\|\mathbf{x}\|^2}{V_{\text{eff}}^2}. \tag{15}$$

For the particular case of the S102G pegleg,

$$\tau_m = \tau^*(y_0 - \mathbf{x}_p/2) \quad \text{and} \quad \tau_p = \tau(y_0 + (\mathbf{x} - \mathbf{x}_p)/2), \tag{16}$$

Relations for other pegleg types are readily derived. Figures 9b and c show that HEMNO can independently flatten each leg of a first-order split salt-related pegleg when the salt geometry obeys HEMNO's dip assumptions.

Implementation of equation (15) requires two quantities: τ_m, obtained by hand or auto-picking, and more challengingly, τ_p, an arbitrary reflector's zero-offset traveltime. We obtain τ_p automatically by event tracking, using measured zero-offset reflector dip, which may be estimated automatically (Fomel 2002), or manually, with picked reflectors and spline interpolation (Brown 2004).

Combined imaging/modeling operator

Now that we have defined a kinematic multiple imaging operator and a suite of amplitude correction operators, we can define $\mathbf{L}_{i,k,m}$. We map the primary image, $\mathbf{m}_0$, into data space ($\mathbf{d}_0$) by applying the adjoint of normal moveout ($\mathbf{N}_0$). We map the pegleg image, $\mathbf{m}_{i,k,m}$, into data space ($\mathbf{d}_{i,k,m}$) by applying the differential geometric spreading correction ($\mathbf{G}_{i,m}$), Snell Resampling ($\mathbf{S}_{i,m}$), HEMNO

($\mathbf{N}_{i,k,m}$), and finally, the reflection coefficient ($\mathbf{R}_{i,k,m}$):

$$\mathbf{d}_0 = \mathbf{N}_0\mathbf{m}_0 = \mathbf{L}_0\mathbf{m}_0, \tag{17}$$

$$\mathbf{d}_{i,k,m} = \mathbf{R}_{i,k,m}\mathbf{N}_{i,k,m}\mathbf{S}_{i,m}\mathbf{G}_{i,m}\mathbf{m}_{i,k,m} = \mathbf{L}_{i,k,m}\mathbf{m}_{i,k,m}. \tag{18}$$

Equation (18) retains distinct computational advantages. Since the operator images peglegs with a vertical stretch, it is efficient to apply (important in iterative inversion), robust to poor crossline sampling (the norm with 3D data), allows the LSJIMP model space to consist of one midpoint location only (advantageous for parallel computing), which allows the amplitude component of the operator to be intuitive and effective. However, this pegleg modeling/imaging strategy begins to break down when reflectors dip strongly ($> 5°$), dips change rapidly, and in the presence of large velocity contrasts. It cannot model diffracted multiples. It ignores the relative shift in reflection point of a primary and the primary bounce of a pegleg.

Extension to 3D

A common geometry for 3D marine "spec" data consists of sail line spacing chosen just small enough to ensure even crossline midpoint coverage. Ignoring cable feathering, the crossline offset axis in this geometry contains only one live bin per CMP gather, so a CMP gather is effectively two-dimensional, allowing us to reduce the size of the LSJIMP model space by the number of crossline offset bins and greatly speeding up our LSJIMP implementation's performance. Note that we are still imaging the multiples in a 3D sense, since HEMNO a) uses reflector geometries measured from a 3D zero-offset section, and b) we supply the nonzero crossline offset of the assumed "2D" CMP gathers.

FIELD DATA RESULTS

WesternGeco released 2D data from Mississippi Canyon, Gulf of Mexico, for multiple suppression benchmarking. Figure 11 shows that the data contain a variety of strong surface-related multiples which hamper interpretation.

Multiple prediction benchmark

We can use our multiple imaging/modeling operator to predict multiples, given a prior estimate of the primaries, similar to the crosstalk prediction of equation (6). A simple primary estimate comes by applying NMO to the data: $\mathbf{N}_0^T\mathbf{d}$. The predicted multiples, $\mathbf{d}_{\text{mult}}$, are computed by modeling each pegleg and summing:

$$\mathbf{d}_{\text{mult}} = \sum_{i=1}^{p}\sum_{k=0}^{i}\sum_{m=1}^{n_{\text{surf}}}\mathbf{R}_{i,k,m}\mathbf{N}_{i,k,m}\mathbf{S}_{i,m}\mathbf{G}_{i,m}\mathbf{N}_0^T\mathbf{d}. \tag{19}$$

To benchmark the accuracy of our multiple imaging/modeling operator against an industry standard, in Figures 12 and 13 we compare equation (19)'s predicted multiples with those predicted by one convolution of the Surface-Related Multiple Elimination (SRME) method (Verschuur et al. 1992) on the 2D Mississippi Canyon field data.

Figure 12 shows a CMP gather with strong top of salt multiples, including the train of split peglegs between $\tau = 4.0$ and 4.3 seconds. Both approaches accurately model the multiple splitting. Our method's predicted multiples generally reproduce the offset-dependent amplitude and wavelet of the multiples in the data. Figure 13 shows a medium-offset slice. SRME accurately predicts the split peglegs. Our method performs well in some areas (circle), but underperforms (tall oval) where dips steepen or change rapidly. SRME predicts diffracted events (flat oval) which our method does not.

These examples show that away from complex geology, our multiple imaging/modeling strat-

egy can accurately transform primaries into events resembling pegleg multiples. It follows that our method can transform pegleg multiples into events comparable with primaries – a principal criterion that any LSJIMP multiple imaging/modeling pair must satisfy.

2D LSJIMP Field Data Results

We tested our particular LSJIMP implementation on 750 CMPs of the 2D data, modeling only first-order multiples from the four labeled multiple generators in Figure 11 ($p = 1, n_{\text{surf}} = 4$ in equation (1)). We ran twenty conjugate gradient iterations.

Figure 14 shows stacks of the raw data after NMO, the LSJIMP estimated primary image ($\mathbf{m}_0$), and the difference between the two. LSJIMP cleanly separates primaries from a variety of surface-related multiples. However, much subsalt (midpoints $>$ 6000 m) multiple energy remains, for a variety of reasons, especially salt rugosity, which causes diffracted multiples and complex focusing, neither of which HEMNO can handle. Still, our LSJIMP implementation effectively removes the specular components of most strong salt-related multiples without harming primaries. In general, increasing the tradeoff parameters ϵ_1, ϵ_2, and ϵ_3 in equation (7) removes more multiple energy from $\mathbf{m}_0$, at the cost of harming primary signal.

Figure 15 shows prestack LSJIMP results at a single CMP location over the salt (midpoint = 9150 m). Panels 15c, d, g, and h show the estimated total first order pegleg from the seabed, R1, R2, and top of salt reflectors, respectively. The modeled data (Panel 15e) is the sum of the estimated primaries (Panel 15b) and Panels 15c, d, g, and h. The residual error (Panel 15f) is the difference between the input data and modeled data. For example, to compute the estimated seabed pegleg (Panel 15c), we construct a vector,

$$\mathbf{m}_{\text{wb}} = \begin{bmatrix} \mathbf{0} & \mathbf{m}_{1,0,1} & \mathbf{m}_{1,1,1} & \mathbf{0} & \mathbf{0} & \mathbf{0} & \mathbf{0} & \mathbf{0} & \mathbf{0} \end{bmatrix}^T, \tag{20}$$

where vector $\mathbf{0}$ has the same dimension as a CMP gather and $\mathbf{m}_{1,0,1}$ and $\mathbf{m}_{1,1,1}$ are the seabed source and receiver pegleg images. We apply the LSJIMP forward model to compute the total first-order seabed pegleg:

$$\mathbf{d}_{\text{wb}} = \mathbf{L}\mathbf{m}_{\text{wb}}. \tag{21}$$

Since there are no flat events on the residual Panel 15f, we conclude that LSJIMP preserves obscured primaries, like those seen between 3.5 and 4.0 seconds on Panel 15b. Comparing Panels 15a and e, note that even the complex, visibly split salt-related multiples are modeled and separated fairly well. However, the multiples remaining on the residual panel imply that the forward model has not perfectly modeled the physics of the multiples. Notice that the LSJIMP model regularization operators have interpolated the data's missing near offset information.

Figure 16 compares the results of LSJIMP and least-squares high-resolution Radon demultiple (see Trad et al. (2003) for a review) on the CMP gather at the same location as in Figure 15. The high apparent velocity of one leg of the split top of salt pegleg (circled on Panel 16b) significantly degrades Radon's ability to attenuate it. LSJIMP directly models splitting behavior of the event, and can thus better separate it from the estimated primaries.

3D LSJIMP Field Data Results

CGG acquired a 3D speculative survey in the Gulf of Mexico's Green Canyon. We processed a small subset (192 by 14 CMP locations) with nontrivial crossline dip ($> 3°$), extracted from a sedimentary "minibasin". As noted earlier, we ignore the data's crossline offset axis, leaving a four-dimensional prestack data cube and strongly accelerating LSJIMP's performance.

Figure 17 zooms into the multiple-infested zone before and after LSJIMP. Stacking mostly suppresses multiples, but from the difference panel, note that LSJIMP nonetheless subtracts much re-

maining multiple energy without seriously harming primaries. The timeslice on the 3D cube transects a strong seabed pegleg; it shows up prominently on the raw data stack and the difference panel, but is largely absent from the LSJIMP estimated primaries stack.

Figure 18 shows LSJIMP's performance on a CMP gather (for a single nonzero crossline offset). Note strong multiples at $\tau = 4.3$ sec in the raw data (Panel 18a), and primaries under the multiple curtain. The LSJIMP estimated primaries (Panel 18b) are effectively free of multiples, and moreover, since the data residual (Panel 18f) contains little correlated energy, we have preserved the primaries and effectively modeled the data's important multiples (Panels 18c and d).

CONCLUSIONS

We introduced the LSJIMP (Least-squares Joint Imaging of Multiples and Primaries) method, a general least-squares inversion algorithm to simultaneously combine images of the multiples and primaries and suppress the crosstalk noise that inhibits simple image averaging. LSJIMP's novelty lies in the three model regularization operators that suppress crosstalk and exploit the redundancy within and between images to increase signal fidelity.

We presented a particular LSJIMP implementation which used a relatively simple time-domain true-relative-amplitude imaging operator for pegleg multiples. While our pegleg imaging/modeling scheme is limited to specularly-reflected multiples from mildly-dipping reflectors, we demonstrate on a 2D field data example that our method can accurately model salt-related split peglegs. Moreover, the method is robust to sparse 3D marine geometries and computationally efficient, which is crucial for iterative inversion.

Tests on real 2D and 3D marine field data examples confirm that LSJIMP holds promise as a novel and useful tool in the quest to fully exploit more of the unused information in the seismic wavefield.

In both cases, LSJIMP separates primaries from a variety of surface-related pegleg multiples. While the separation is not perfect, the amplitude of primaries is nonetheless preserved. Information from the multiples was shown to help constrain missing near-offset primary information. On the 2D example we compared LSJIMP to high-resolution hyperbolic Radon demultiple and found that LSJIMP separated a split salt-related pegleg from the data better than Radon demultiple.

Looking toward the future, we note that the continued trend toward inexpensive parallel computing may soon allow LSJIMP implementations with more accurate (and expensive) prestack imaging operators for multiples. LSJIMP shows great promise to jointly image other important wave modes often seen in the data. Local shear wave conversions (Purnell 1992) and internal multiples may offer valuable information in the subsalt imaging problem; these modes fit the "one data record, many datasets" model of LSJIMP. Extensions to LSJIMP for multicomponent data are possible.

ACKNOWLEDGMENTS

Thanks go to WesternGeco and CGG for acquiring and releasing the field data shown in this paper, as well as the sponsors of the Stanford Exploration Project for financial and technical support. This work benefited from useful discussions and support from Robert Clapp, Biondo Biondi, and Clement Kostov, as well as from thoughtful and patient reviews by the Associate Editor and two anonymous reviewers.

REFERENCES

Berkhout A. and Verschuur D. 2003. Transformation of multiples into primary reflections: 73rd Annual International Meeting, SEG, Expanded Abstracts, 1925–1928.

Berkhout A.J. and Verschuur D.J. 1994. Multiple technology: Part 2, migration of multiple reflections: 64th Annual International Meeting, SEG, Expanded Abstracts, 1497–1500.

Berryhill J.R. and Kim Y.C. 1986. Deep-water peglegs and multiples - Emulation and suppression: Geophysics, **51**, 2177–2184.

Brown M.P. 2004. Least-squares joint imaging of multiples and primaries: Ph.D. thesis, Stanford University.

URL : `http://sepwww.stanford.edu/public/docs/sep116/paper_html/`

Claerbout J.F. 1992. Earth Soundings Analysis: Processing Versus Inversion: Blackwell Scientific Publications.

Fomel S. 2002. Applications of plane-wave destruction filters: Geophysics, **67**, 1946–1960.

Guitton A. 2002. Shot-profile migration of multiple reflections: 72nd Annual International Meeting, SEG, Expanded Abstracts, 1296–1299.

Guitton A., Brown M., Rickett J. and Clapp R. 2001: Multiple attenuation using a t-x pattern-based subtraction method: 71st Annual International Meeting, SEG, Expanded Abstracts, 1305–1308.

He R. and Schuster G. 2003. Least-squares migration of both primaries and multiples: 73rd Annual International Meeting, SEG, Expanded Abstracts, 1035–1038.

Kuehl H. and Sacchi M. 2001. Generalized least-squares DSR migration using a common angle imaging condtion: 71st Annual International Meeting, SEG, Expanded Abstracts, 1025–1028.

Levin F.K. and Shah P.M. 1977. Peg-leg multiples and dipping reflectors: Geophysics, **42**, 957–981.

Lu G., Ursin B. and Lutro J. 1999. Model-based removal of water-layer multiple reflections: Geophysics, **64**, 1816–1827.

Morley L. 1982. Predictive Multiple Suppression: Ph.D. thesis, Stanford University.

URL : http://sepwww.stanford.edu/oldreports/sep29/index.html

Nemeth T., Wu C. and Schuster G.T. 1999. Least-squares migration of incomplete reflection data: Geophysics, **64**, 208–221.

Prucha-Clapp M. and Biondi B. 2002. Subsalt event regularization with steering filters: 72nd Annual International Meeting, SEG, Expanded Abstracts, 1176–1179.

Purnell G.W. 1992. Imaging beneath a high-velocity layer using converted waves: Geophysics, **57**, 1444–1452.

Reiter E.C., Toksoz M.N., Keho T.H. and Purdy G.M. 1991. Imaging with deep-water multiples: Geophysics, **56**, 1081–1086.

Riley D.C. and Claerbout J.F. 1976. 2-D multiple reflections: Geophysics, **41**, 592–620.

Ross W.S., Yu Y. and Gasparotto F.A. 1999. Traveltime prediction and suppression of 3-D multiples: Geophysics, **64**, 261–277.

Sava P. and Fomel S. 2003. Angle-domain common-image gathers by wavefield continuation methods: Geophysics, **68**, 1065–1074.

Shan G. 2003. Source-receiver migration of multiple reflections: 73rd Annual International Meeting, SEG, Expanded Abstracts, 1008–1011.

Tarantola A. 1987. Inverse Problem Theory: Methods for Data Fitting and Model Parameter Estimation: Elsevier.

Trad D., Ulrych T. and Sacchi M. 2003. Latest views of the sparse Radon transform: Geophysics, **68**, 386–399.

Tsai C.J. 1985. Use of autoconvolution to supress first-order long-period multiples: Geophysics, **50**, 1410–1425.

Verschuur D.J., Berkhout A.J. and Wapenaar C.P.A. 1992. Adaptive surface-related multiple elimination: Geophysics, **57**, 1166–1177.

Wang J., Kuehl H. and Sacchi M. 2003. Least-squares wave-equation AVP imaging of 3D common azimuth data: 73rd Annual International Meeting, SEG, Expanded Abstracts, 1039–1042.

Wang Y. 2003. Multiple subtraction using an expanded multichannel matching filter: Geophysics, **68**, 346–354.

Wiggins J.W. 1988. Attenuation of complex water-bottom multiples by wave equation-based prediction and subtraction: Geophysics, **53**, 1527–1539.

Yu J. and Schuster G. 2001. Crosscorrelogram migration of IVSPWD data: 71st Annual International Meeting, SEG, Expanded Abstracts, 456–459.

LIST OF FIGURES

alent to "pseudo-primary" with extra zero-offset traveltime τ^*.

7 A primary and pegleg multiple with the same emergence angle (θ) and midpoint (y).

8 (a): Synthetic CMP gather after NMO. Note two dead and five unrecorded near-offset traces. (b): after NMO for first-order seabed peglegs and (normalized) Snell Resampling.

9 (a): Real CMP gather with split first-order top of salt pegleg (labels indicate the two legs). Pegleg apexes shift away from zero offset. (b) and (c): HEMNO (plus previous amplitude corrections) applied to the two legs.

10 HEMNO schematic. (a): True S102G pegleg raypath. (b): Assumed 1D earth reflection points. (c): Stretch raypath vertically to match measured $\tau^*(y_0 - x_p/2)$ and $\tau(y_0 + (\mathbf{x} - \mathbf{x}_p)/2)$. (d): Connect legs of composite raypath; solid line is final result.

11 Stacked 2D GoM data, after AGC. Picks denote the four multiple generators (seabed - WB, R1, R2, and top of salt - TS). Naming convention for pure multiples: (*reflector*)M (e.g., WBM) and for pegleg multiples: (*target*)PL(*multiple generator*) (e.g., TSPLWB).

12 Left: raw CMP gather (CMP=9150 m). Center: Our predicted multiples. Right: SRME predicted multiples.

13 Left: raw medium-offset section. Center: Our predicted multiples. Right: SRME predicted multiples.

14 Stacked images before and after LSJIMP. All panels gained with t^2 and clipped to same level. (a): Raw data. (b): LSJIMP estimated primaries ($\mathbf{m}_0$). (c): Difference.

15 2D GoM CMP 344 (9150 m) before and after LSJIMP. Panels defined in text. All panels NMO'ed, windowed from 3.5 to 5.5 seconds, and gained with t^2 for ease of viewing.

16 LSJIMP versus least-squares high-resolution hyperbolic radon demultiple on CMP 344 (9150 m) of the Mississippi Canyon 2D dataset. (a): Raw data. (b): radon estimated primaries. (c): radon estimated multiples. (d): LSJIMP estimated primaries. (e): LSJIMP estimated multiples.

17 Zoom of stacked subset of CGG 3D data before and after LSJIMP. All panels windowed in time from 4.0 to 5.0 seconds. Left: Raw data stack. Center: Stack of estimated primary image, $\mathbf{m}_0$. Right: Stack of the subtracted multiples.

18 LSJIMP results on individual midpoint location (CMPx=100,CMPy=4). Panels defined in text. All panels NMO'ed, windowed in time from 4.0 to 6 sec, and gained with t^2 for ease of viewing.

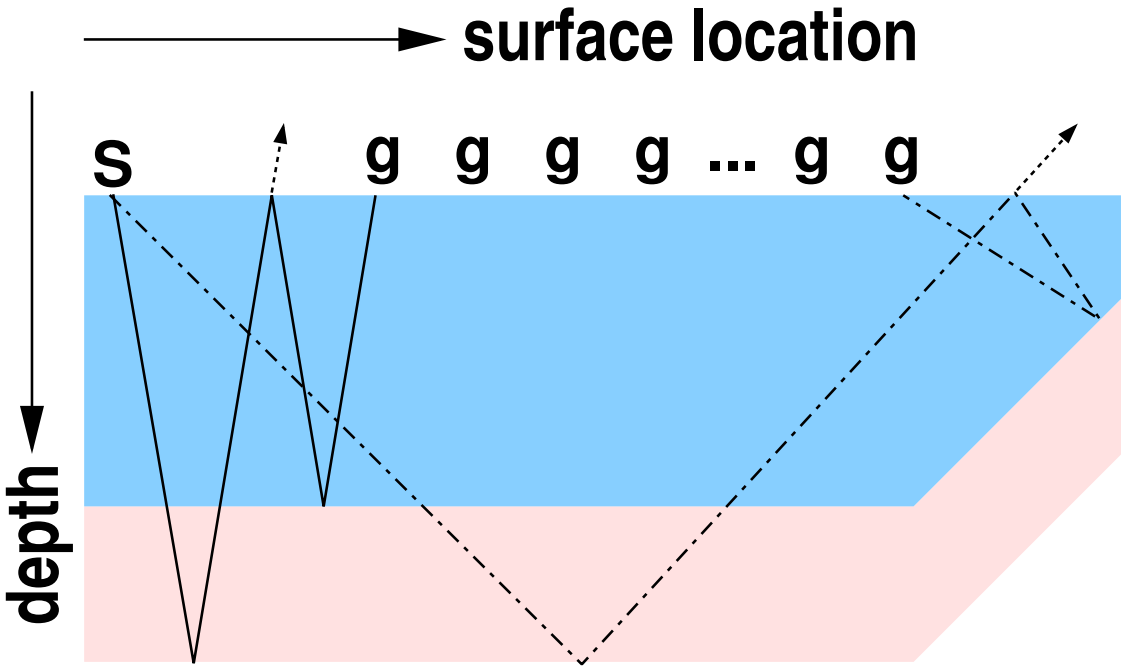

Figure 1.

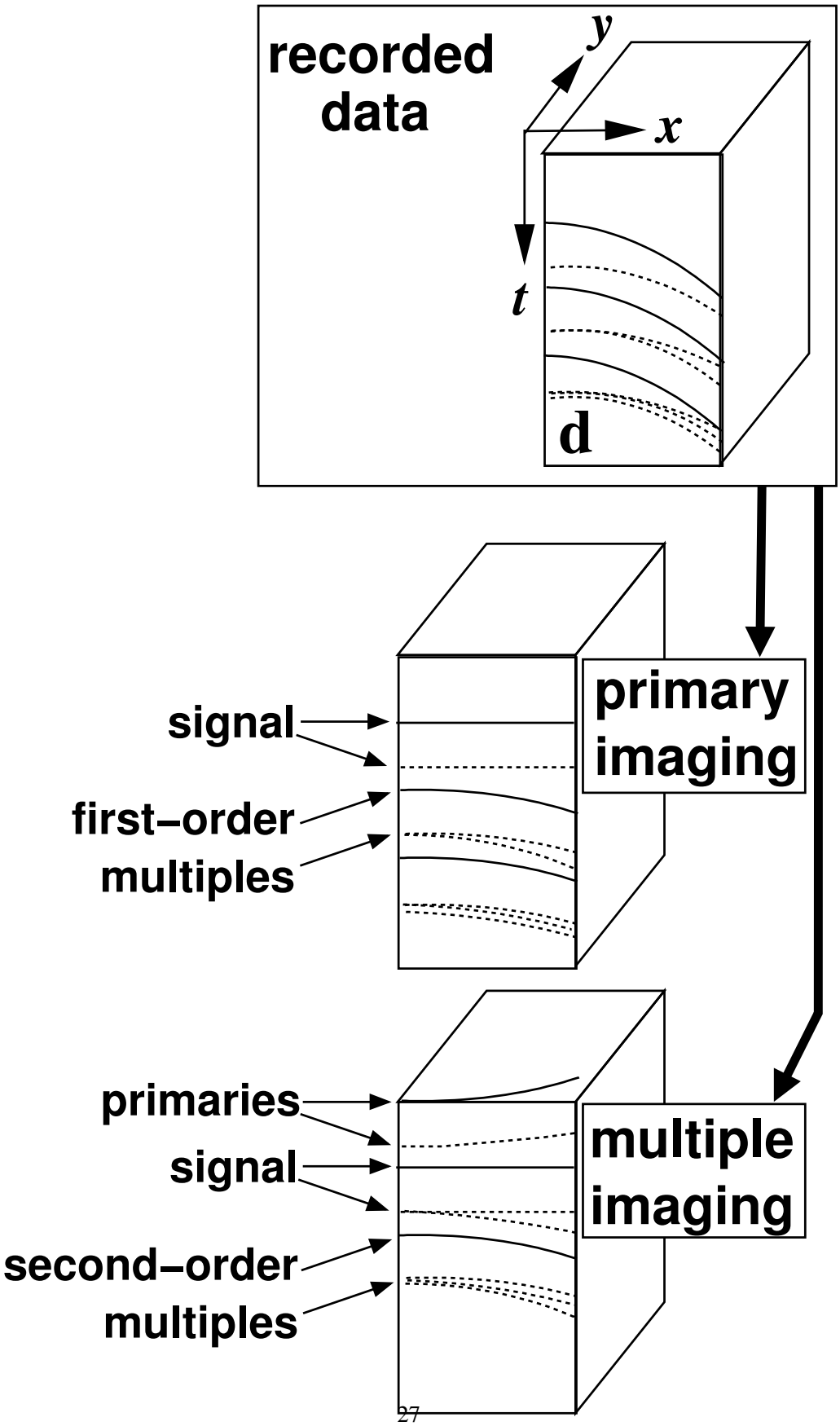
recorded
data
y
x
t
d
primary
imaging
signal
first–order
multiples
multiple
imaging
primaries
signal
second–order
multiples

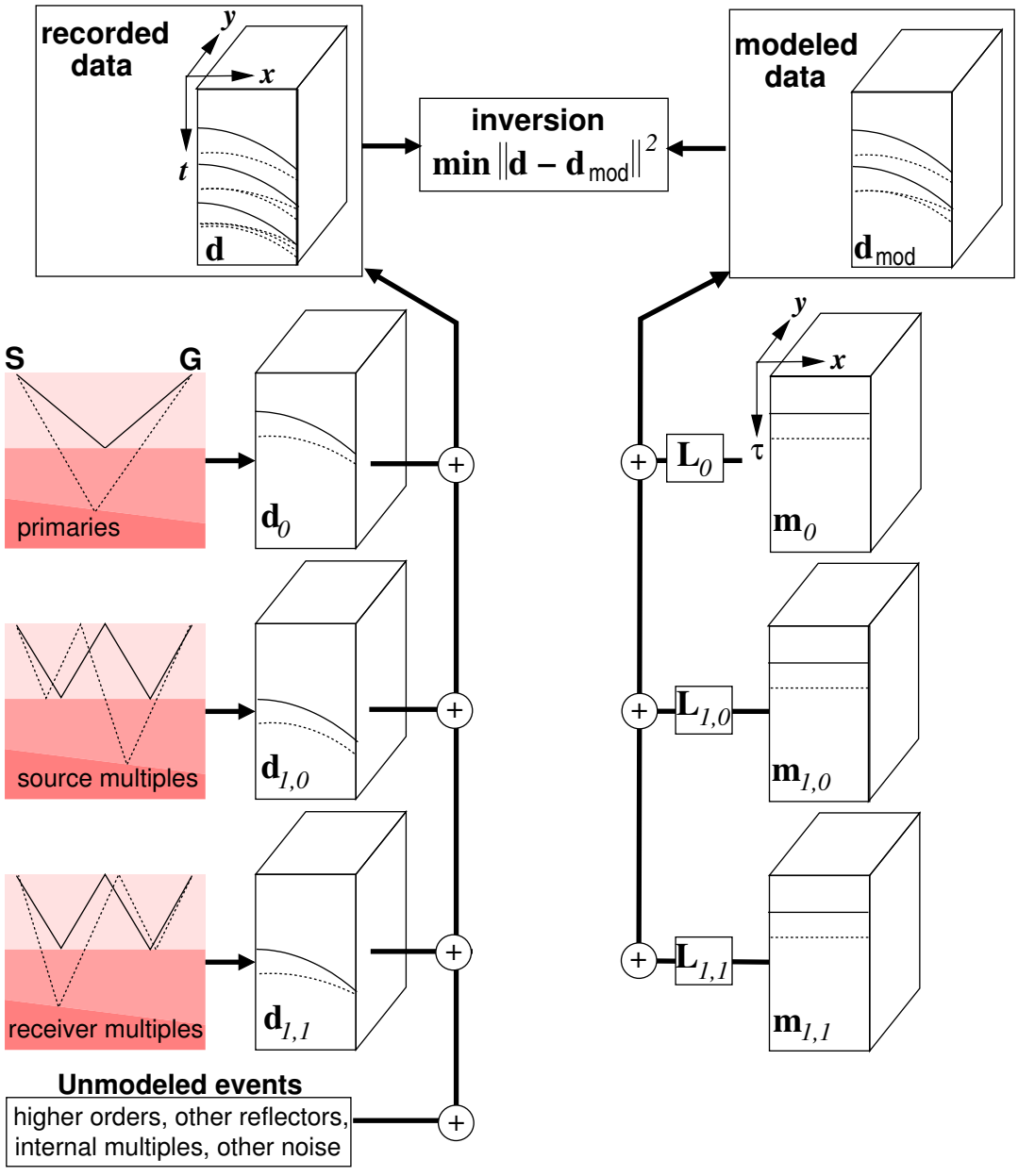
recorded data
y
x
t
d
inversion
min ||d – d mod||2
modeled data
d mod
S
G
primaries
d0
source multiples
d1,0
receiver multiples
d1,1
Unmodeled events
higher orders, other reflectors, internal multiples, other noise
y
x
τ
L0
m0
L1,0
m1,0
L1,1
m1,1

Figure 3.

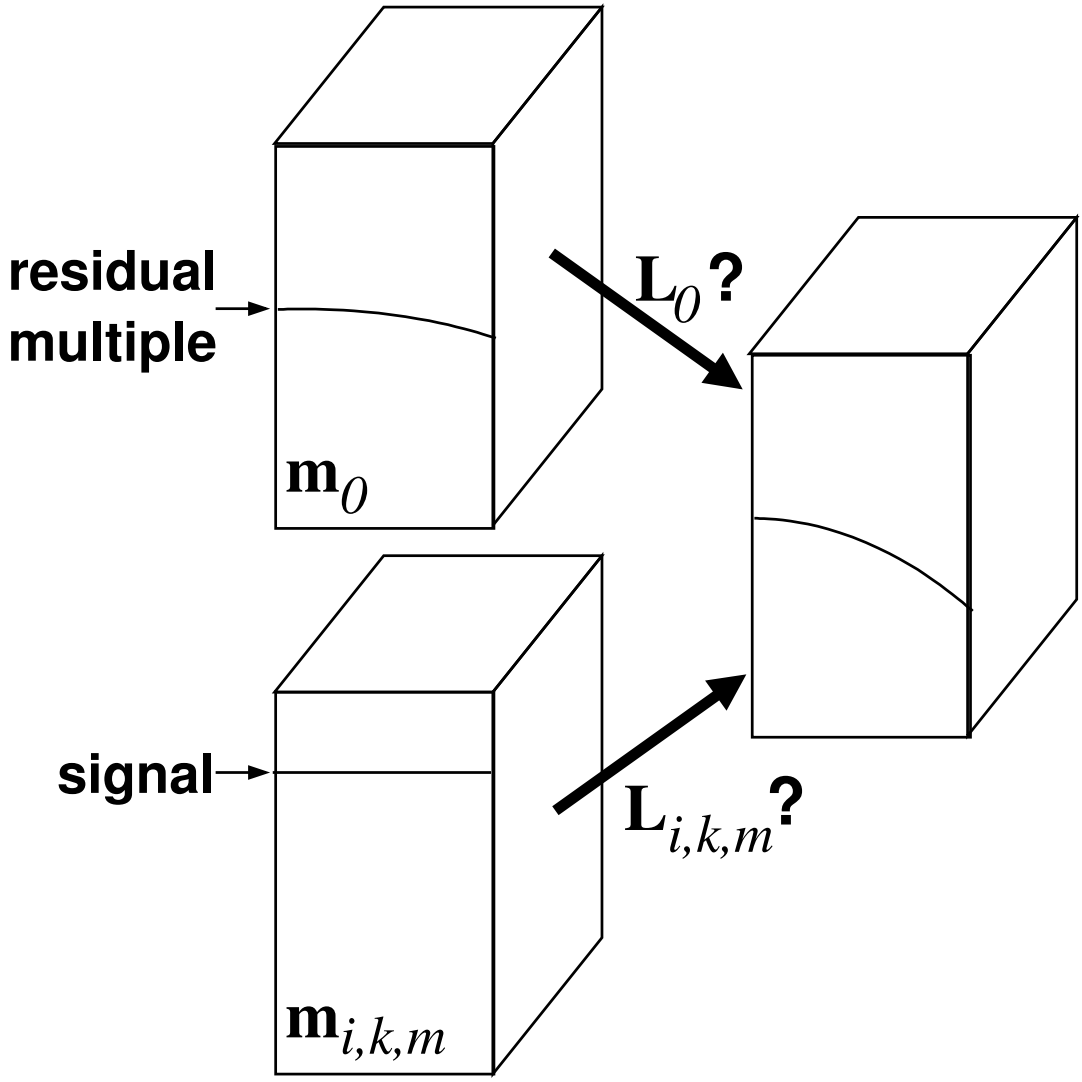
residual
multiple
$\mathbf{m}_0$
$\mathbf{L}_0$?
signal
$\mathbf{m}_{i,k,m}$
$\mathbf{L}_{i,k,m}$?

Figure 4.

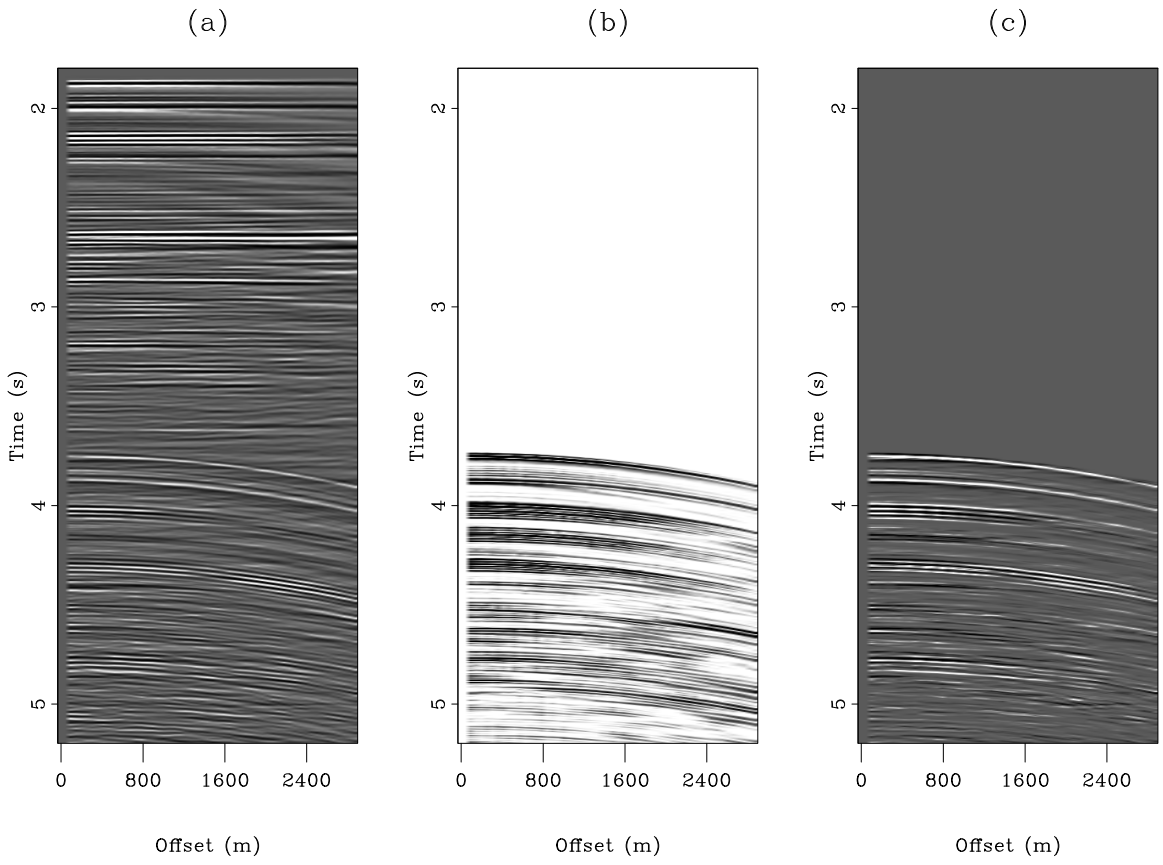

Figure 5.

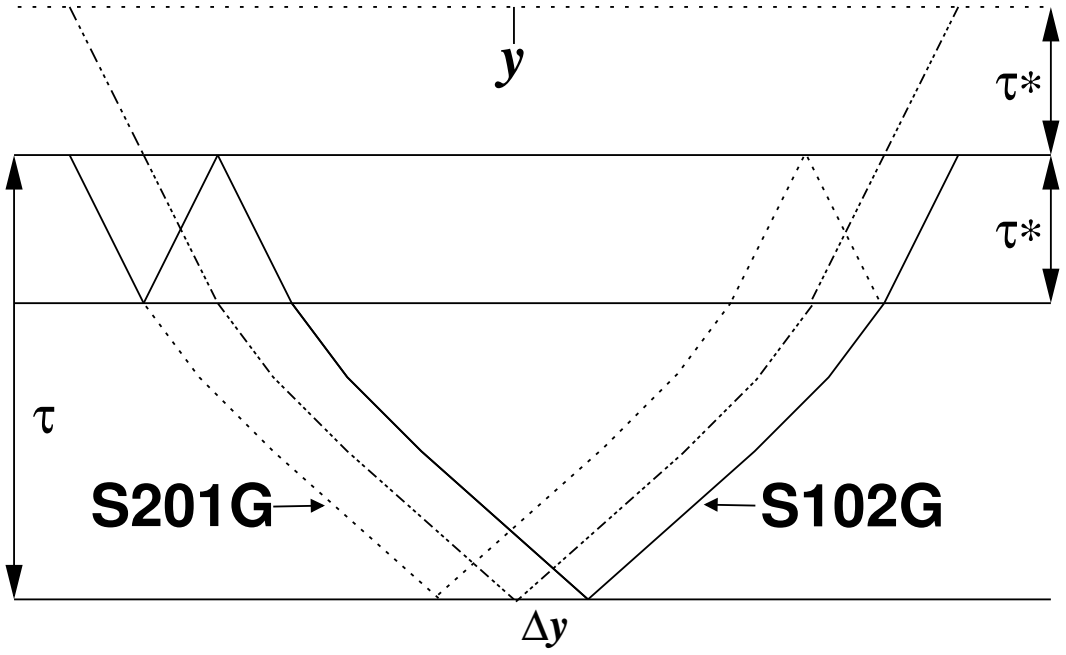

Figure 6.

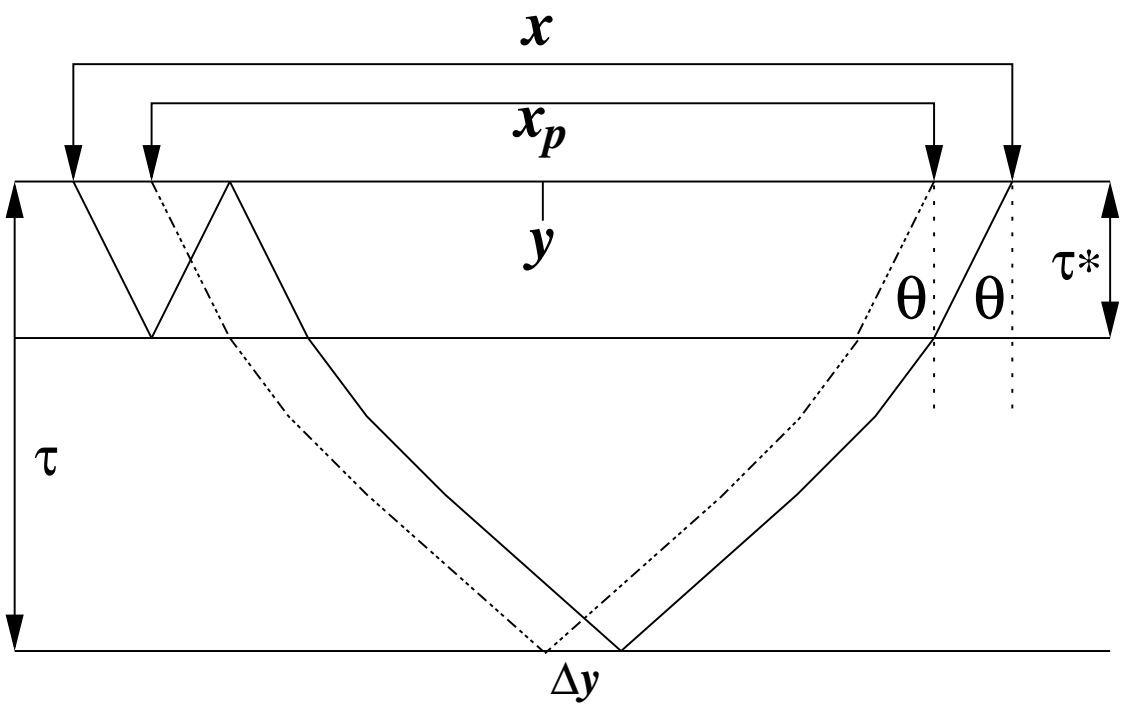

Figure 7.

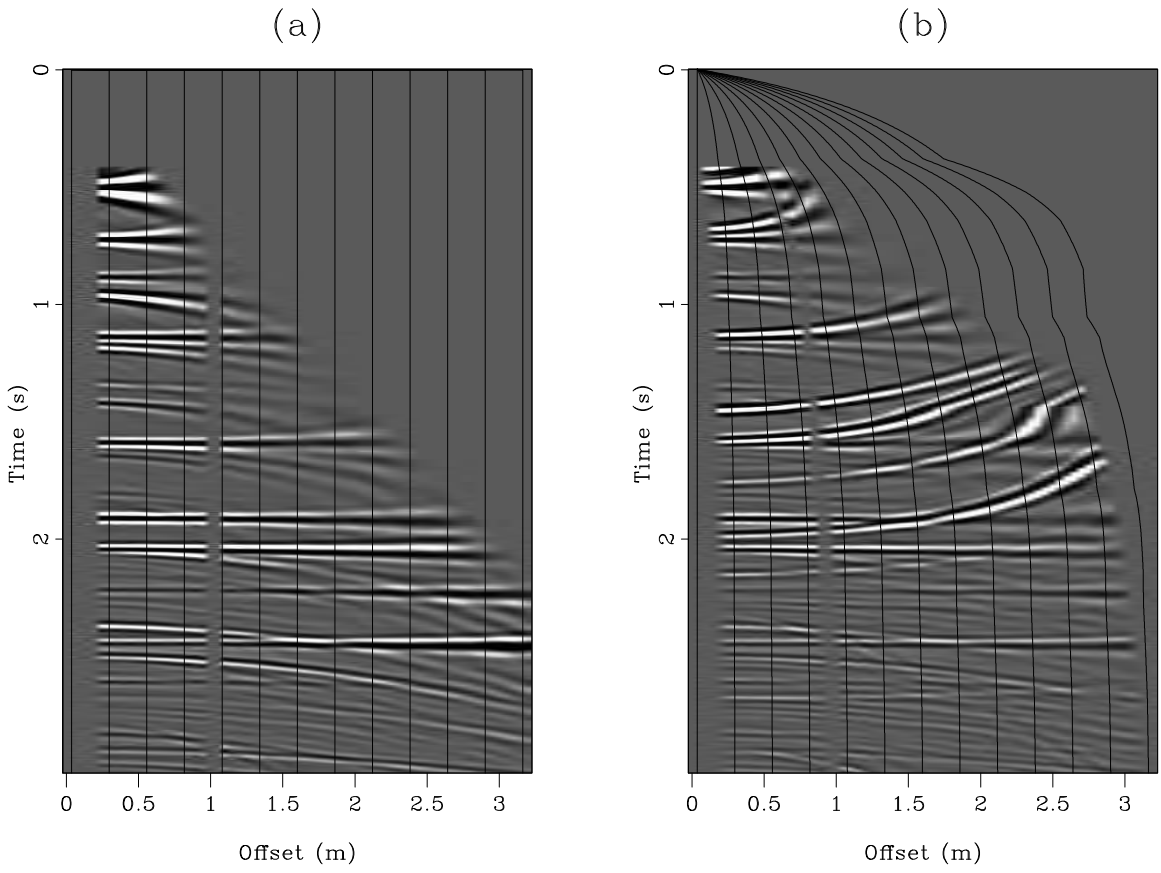

Figure 8.

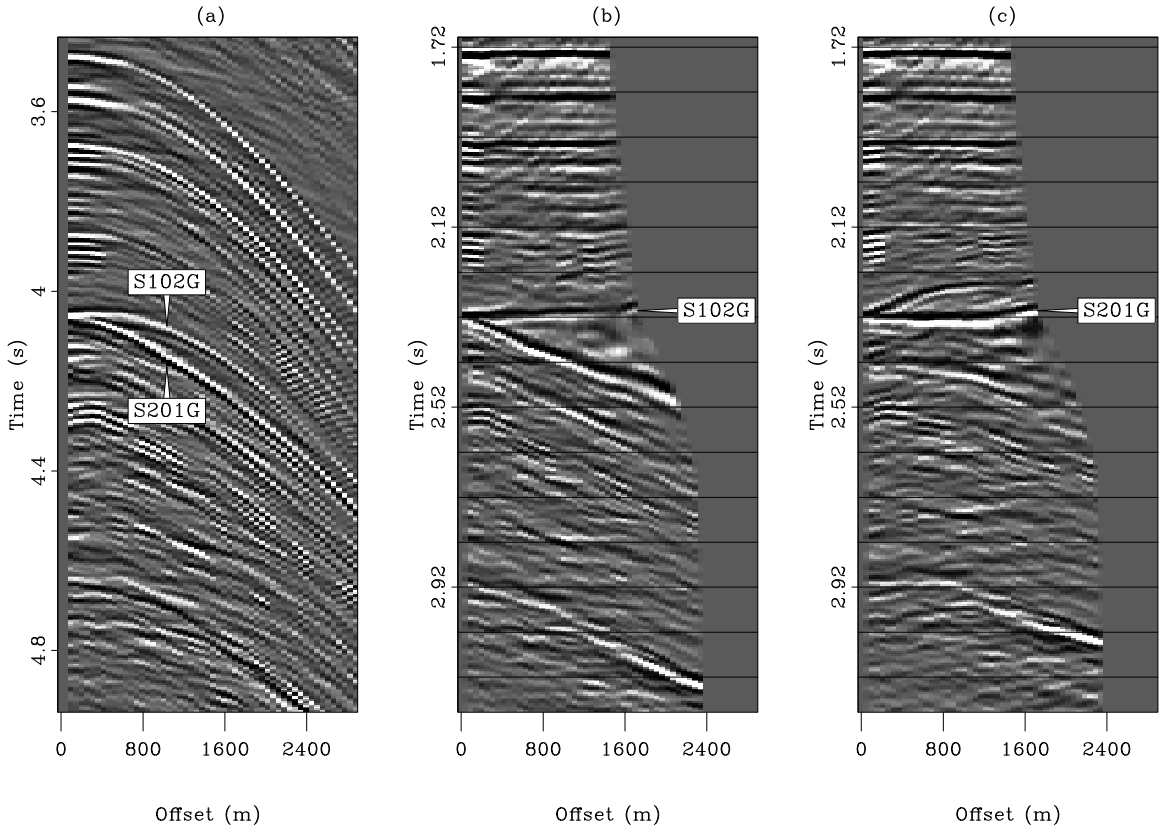
(a)
(b)
(c)
Time (s)
3.6
4
4.4
4.8
1.72
2.12
2.52
2.92
S102G
S201G
0
800
1600
2400
Offset (m)

Figure 9.

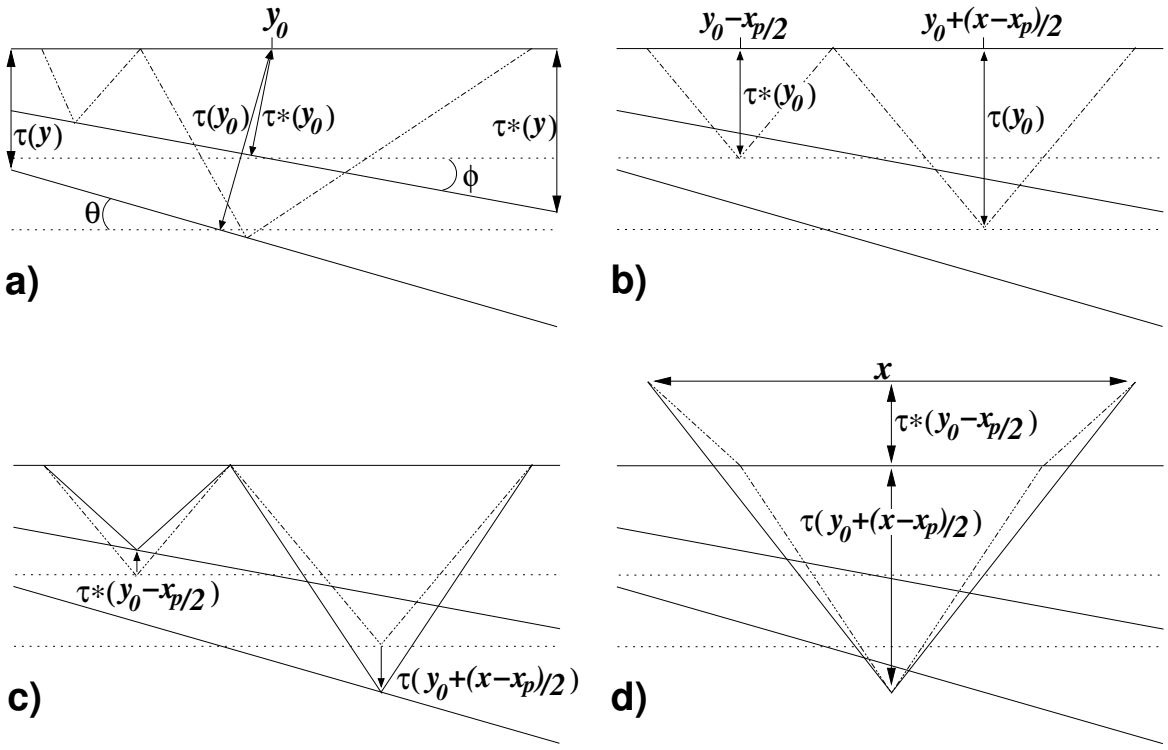
y_0
$\tau(y_0)$
$\tau^*(y_0)$
$\tau(y)$
$\tau^*(y)$
ϕ
θ
a)
$y_0-x_p/2$
$y_0+(x-x_p)/2$
$\tau^*(y_0)$
$\tau(y_0)$
b)
$\tau^*(y_0-x_p/2)$
$\tau(y_0+(x-x_p)/2)$
c)
x
$\tau^*(y_0-x_p/2)$
$\tau(y_0+(x-x_p)/2)$
d)

Figure 10.

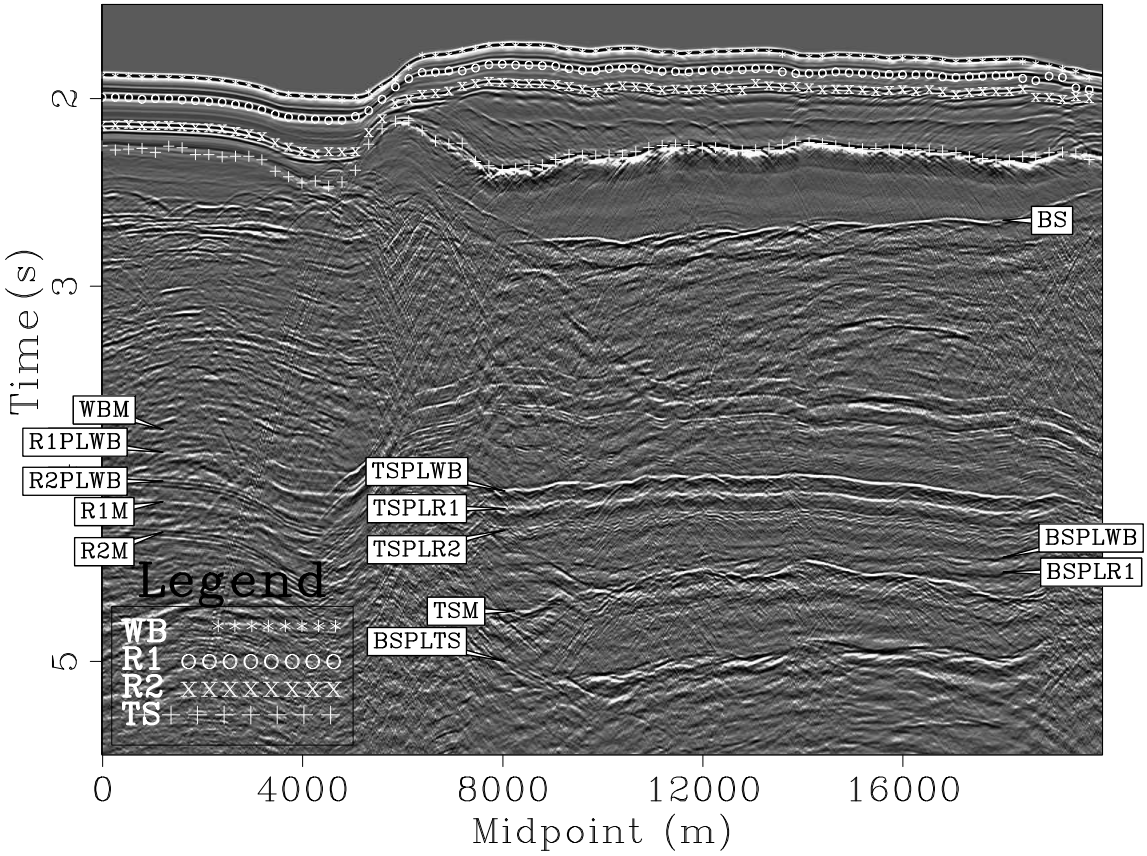
Time (s)
2
3
5
0
4000
8000
12000
16000
Midpoint (m)
BS
WBM
R1PLWB
R2PLWB
R1M
R2M
TSPLWB
TSPLR1
TSPLR2
TSM
BSPLTS
BSPLWB
BSPLR1
Legend
WB
R1
R2
TS

Figure 11.

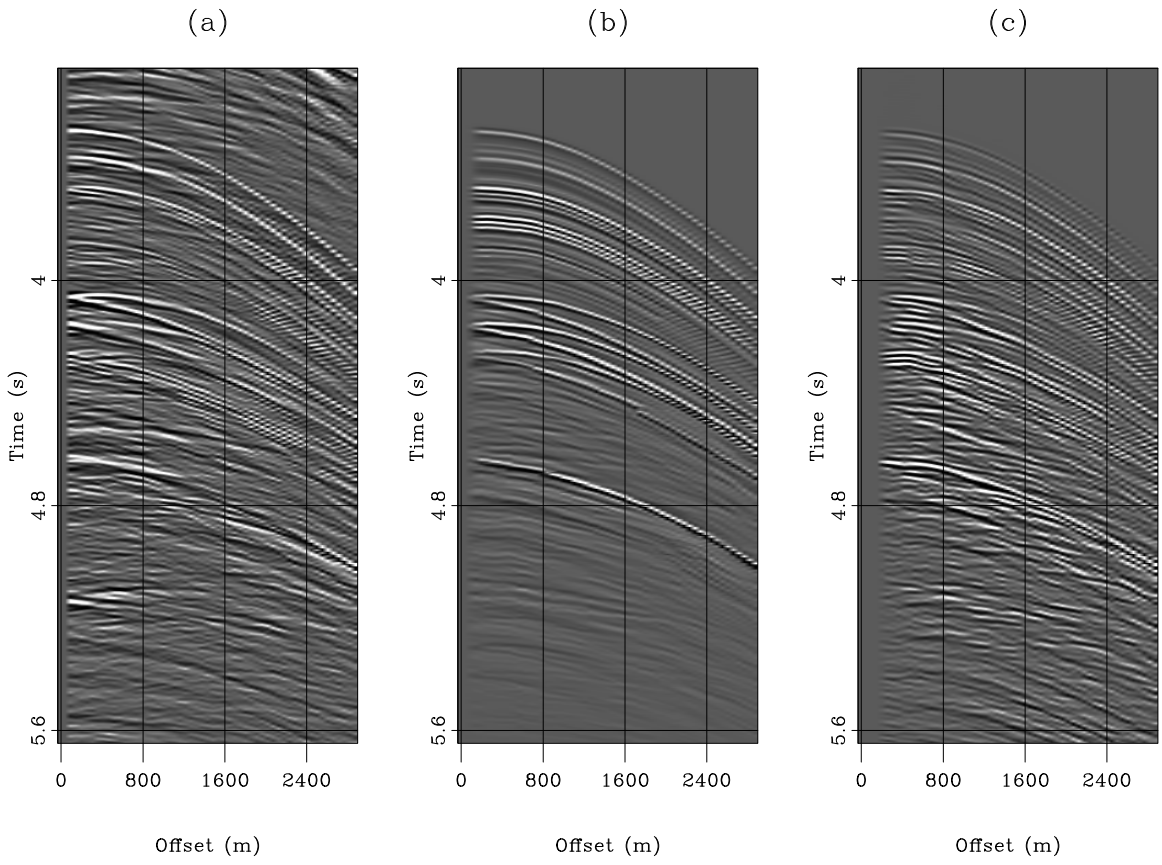

Figure 12.

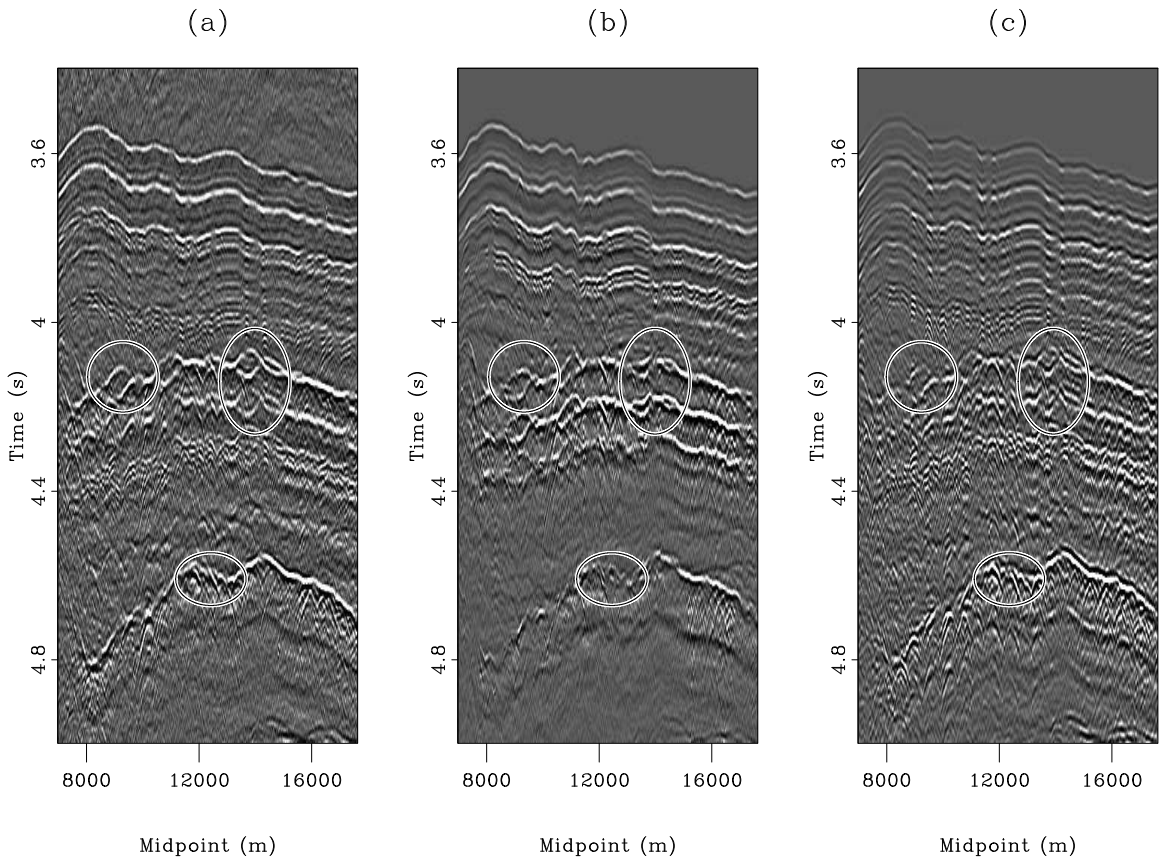

Figure 13.

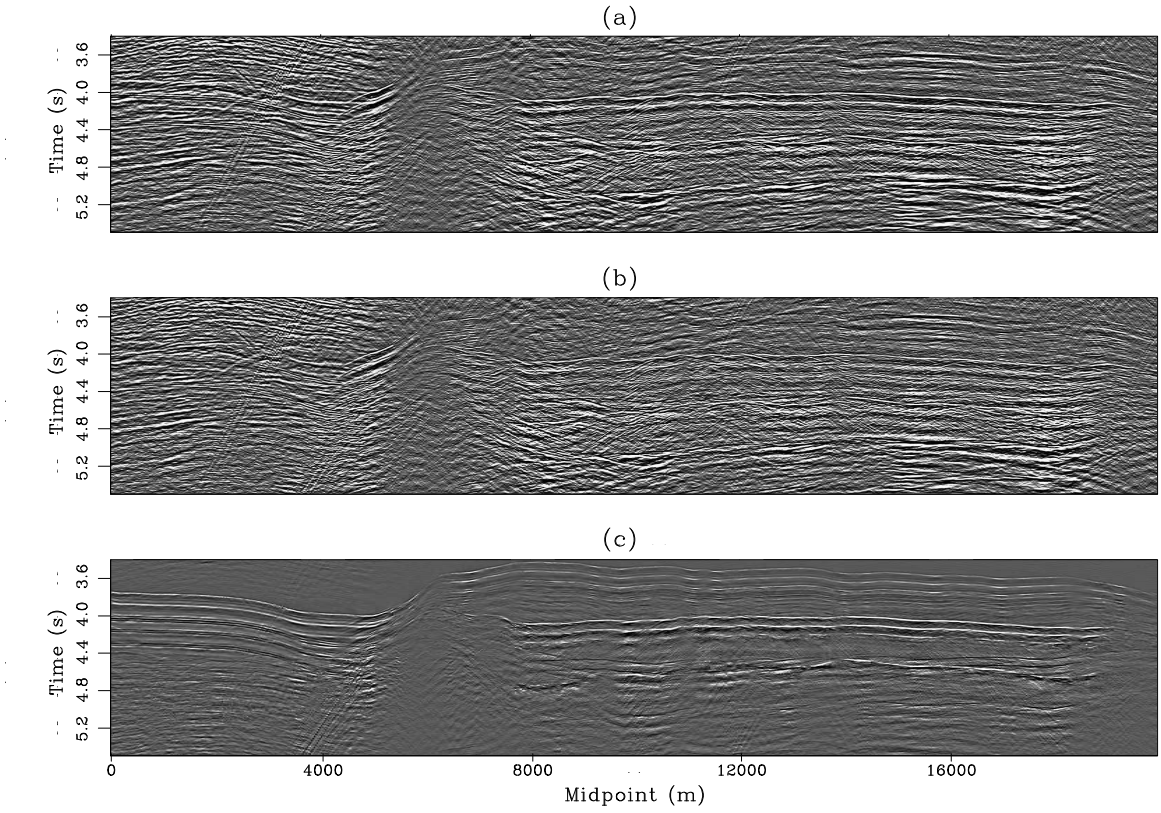
(a)
Time (s)
3.6
4.0
4.4
4.8
5.2
(b)
Time (s)
3.6
4.0
4.4
4.8
5.2
(c)
Time (s)
3.6
4.0
4.4
4.8
5.2
0
4000
8000
12000
16000
Midpoint (m)

Figure 14.

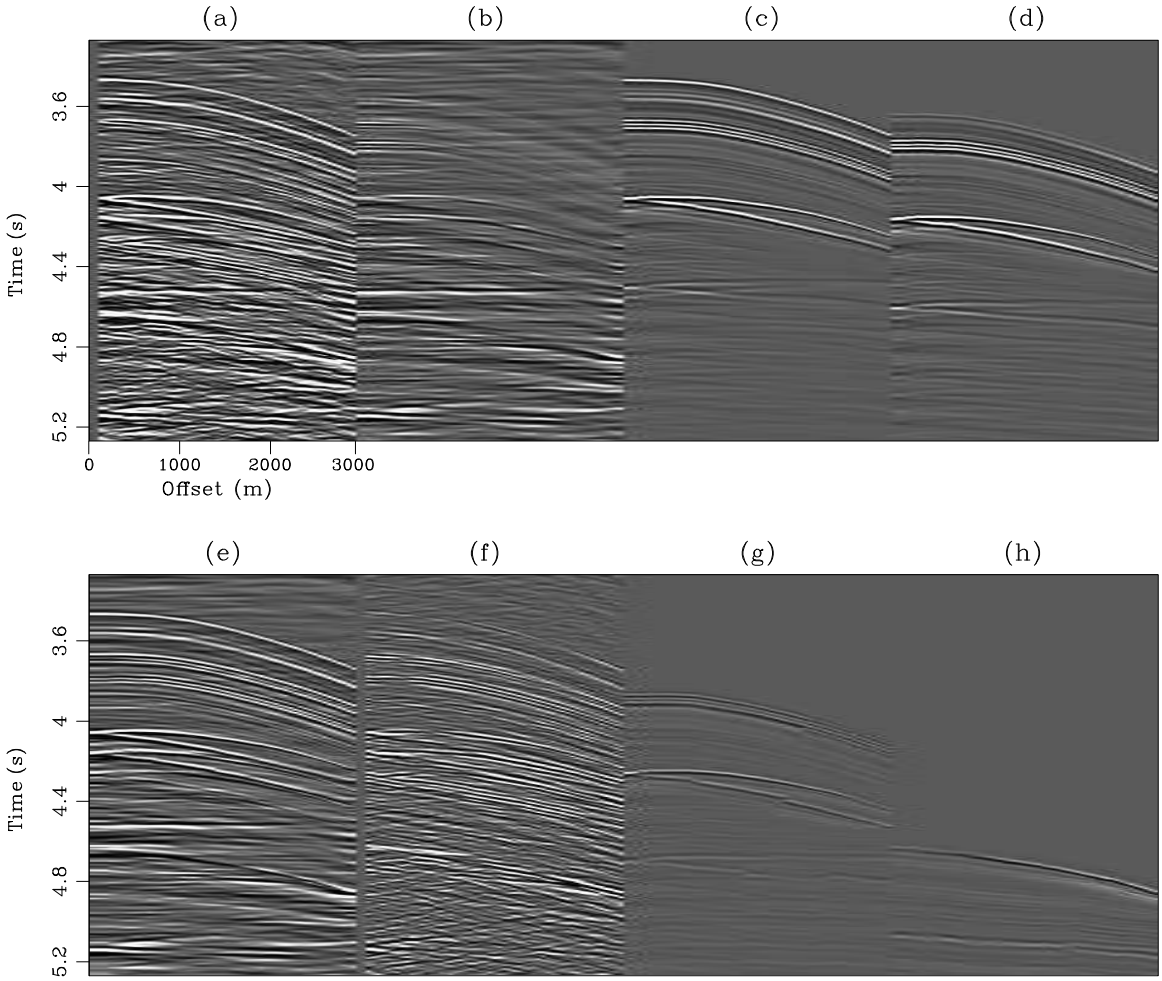

Figure 15.

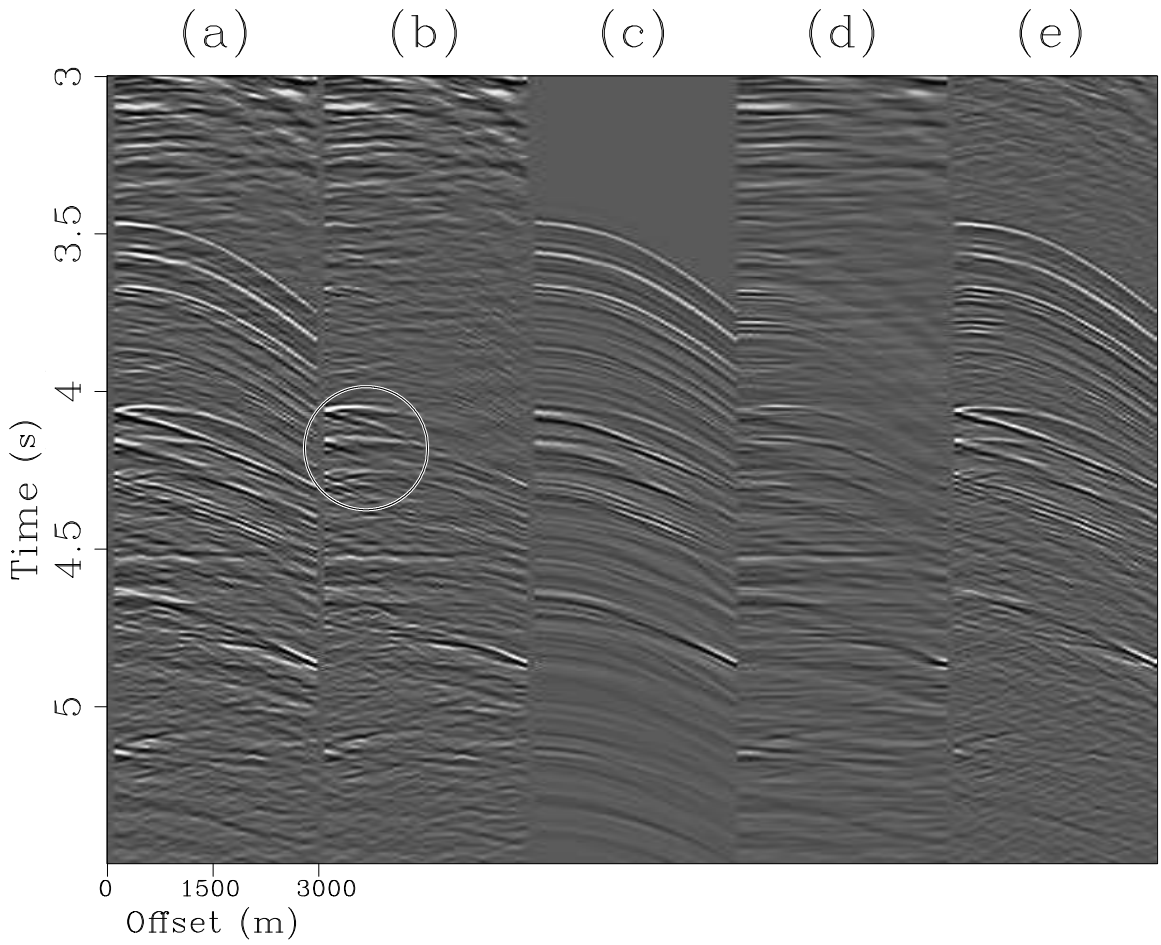

Figure 16.

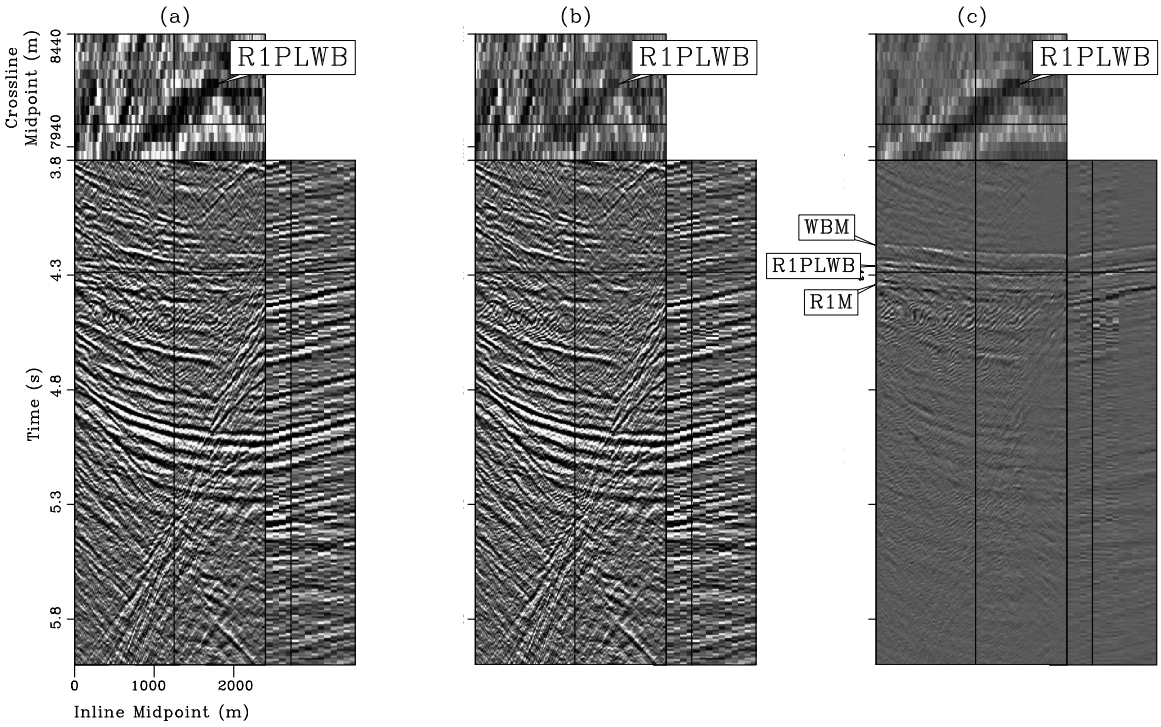
(a)
(b)
(c)
R1PLWB
R1PLWB
R1PLWB
WBM
R1PLWB
R1M
Crossline
Midpoint (m)
8440
7940
Time (s)
3.8
4.3
4.8
5.3
5.8
0
1000
2000
Inline Midpoint (m)

Figure 17.

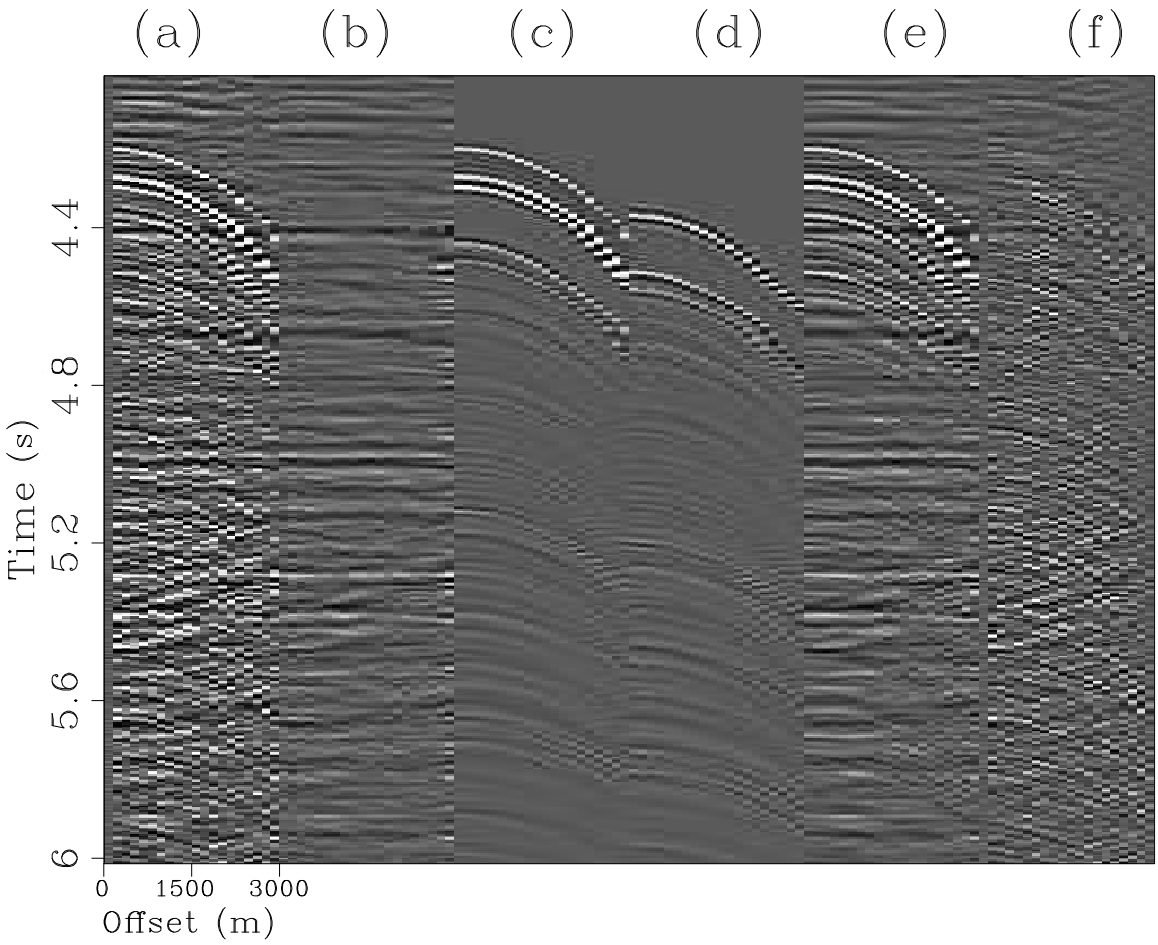

Figure 18.